ACS OMEGA

http://pubs.acs.org/journal/acsodf

Article

Mechanical Properties of Calcium Aluminate Cement Reinforced with Plasma-Treated Basalt Fibers for In Situ Combustion

Hua Zhang, Xiaowei Cheng, Jintang Guo,* Jingxuan Cai, and Xiucheng Ni

Cite This: *ACS Omega* 2023, 8, 1864−1875

Read Online

ACCESS | Metrics & More | Article Recommendations

ABSTRACT: Brittleness and poor tensile/flexural properties restrict the application of calcium aluminate cement (CAC) in oil and gas wells. Reinforcing CAC with fibers is an effective method for improving its strength and toughness and overcoming the shortcomings of its mechanical properties. In this article, as an auxiliary cementing material, slag does not affect the thickening time of CAC. After adding slag, the cement slurry meets the thickening time during cementing construction, and basalt fiber is selected as the toughening material. The enhancement effect of basalt fiber on the mechanical properties of CAC slag composites is studied, including the evaluation of the macroscopic mechanical properties and microstructure at a high temperature (500 °C). The optimum composition of basalt and fiber-reinforced CAC was determined. Basalt fibers were added to CAC at different contents of 0, 0.1, 0.2, 0.3, 0.4, and 0.5% based on the weight of the cement. All the results showed that the introduction of basalt fibers could significantly enhance the strength of the cement at high temperatures. Compared with the control samples, an additional increase in the compressive and tensile strengths of the samples of 35.1 and 85.2%, respectively, was achieved at high temperature with approximately 0.4% fiber content. Plasma treatment further improved the reinforcing effect of the basalt fibers, where the high-temperature compressive and tensile strengths of the samples increased from 28.88 and 1.52 to 35.23 and 1.87 MPa, respectively, an increase of 21.98 and 20.6%, respectively, compared with the untreated basalt fibers. When the cement paste is cured by simulated curing for 28 d, the high-temperature compressive strength and tensile strength with plasma modification increased from 28.26 and 1.5 to 29.1 and 2.15 MPa, respectively, an increase of 3.0 and 43.3%, respectively. The structure of the formed hydrates was studied using scanning electron microscopy. Furthermore, toughening of the basalt fiber-reinforced CAC-based composites resulted mainly from crack bridging and fiber pull-out.

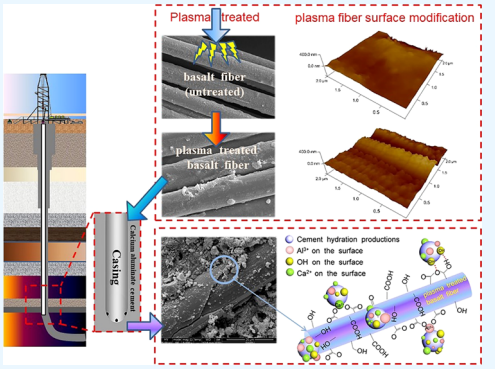

1. INTRODUCTION

Oil-well cementing plays an important role among all operations performed during oil or gas well drilling in the petroleum and gas industry. Oil-well cementing is frequently used to achieve structural integrity and an effective wellbore as well as zonal isolation.[1−3] Currently, heavy oil extraction is one of the severe challenges in the oil and gas industry. In situ combustion (ISC) is currently a more mature means of heat recovery, as shown in Figure 1; it requires the injection of oxidizing gas to produce heat by burning a small fraction of resilient oil and sustaining the combustion front in the reservoir.[4,5] During the thermal recovery of ISC heavy oil, the bearing temperature of the downhole cement ring can reach 500 °C.[6,7] This is also the fixed temperature used in studies of the thermal recovery of heavy oil, and it is the most representative. Thermal deformation and thermal stresses resulting from high temperatures cause cracking, which negatively affects the mechanical behavior and durability of cement composites.[8] Therefore, the thermal stability of cement structures at high temperatures has received considerable attention from researchers in the past few decades.

The use of calcium aluminate cement (CAC) in the petroleum and natural gas industries is a promising way to improve the fire resistance of oil-well cementing compared to the commonly used class G oil-well cement; its advantages are shown in Table 1. Owing to its early strength development and excellent temperature resistance, CAC is often used under the special conditions encountered in the wells.[9] However, cement-based composites are very brittle, and with continuous exposure to higher temperatures, failure of the system related to the downhole cement ring will become more serious, and the system becomes more brittle. To overcome these weaknesses, attempts have been made to reinforce CAC-based composites. To date, many materials have been used for CAC modification, but most

Received: January 30, 2022
Accepted: April 13, 2022
Published: January 3, 2023

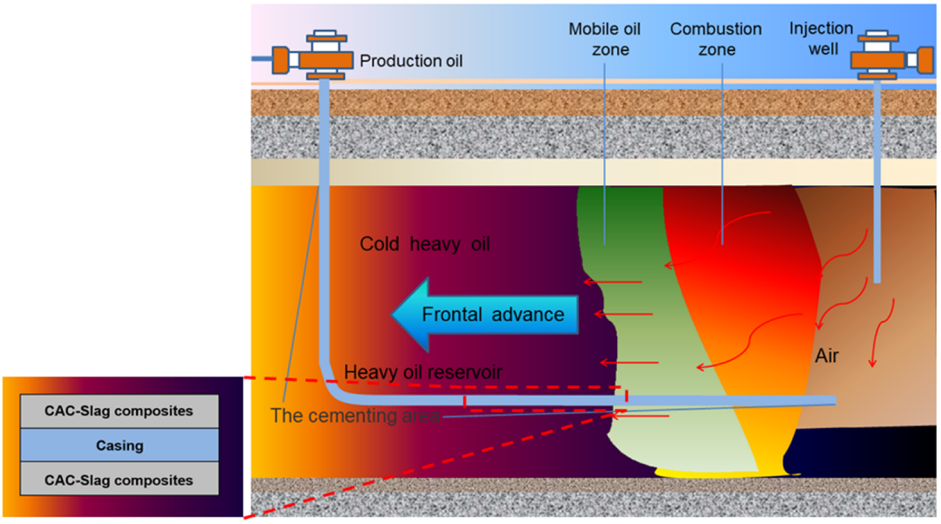

Figure 1. Schematic diagram of thermal recovery of heavy oil.

Table 1. Comparison between This Research Method and Conventional Methods

research methods of this paper	conventional research methods
1. the use of aluminate cement itself has good high-temperature resistance	1. the high-temperature resistance of class G oil-well cement is improved by adding quartz sand. The heat resistance of class G oil-well cement itself is poor
2. the use of slag and modified basalt fiber once again improves the mechanical properties of cement paste at high temperature	2. at ultra-high temperature, the quartz sand adding effect of class G oil-well cement is not significant
3. this method reduces the use of materials and saves costs	3. conventional methods consume a lot of materials and increase the cost

of them are not suitable for cementing oil and gas wells, especially under ultra-high-temperature conditions such as those found in heavy oil ISC wells. Research shows that fibers can be incorporated into the cementitious matrix, and the use of this microfiber reinforcement enhances the mechanical performance of cement composites.[10] It is well known that polymer synthetic fibers,[11] natural fibers,[12,13] carbon fibers,[14] and steel fibers[15] can enhance the ductility and delay crack growth in cement materials. Unfortunately, existing research mainly concentrates on the mechanical properties of CAC at room temperature, which cannot satisfy the demands of application in high-temperature environments. Previous research has shown that steel fiber-modified cement composites are unstable when used in humid environments,[16] and carbon fiber is prohibitively expensive. Hence, it is necessary to choose a suitable external admixture that is highly compatible with cement-based materials to meet the demands of high-temperature operation.

Studies have shown that the use of low-temperature plasma treatment can enhance the reinforcing effect of fibers.[17−19] Basalt fibers (BFs), which are fabricated by melting the basalt rock and extruding the molten rock through a nozzle, can be produced by a simple process and are inexpensive.[20] Further, BFs exhibit excellent tensile strength and stress strength compared with glass fiber and carbon fiber.[21] BFs can also reduce the generation and growth of microcracks and have been used as unique reinforcing materials in cement composites. Moreover, compared to synthetic fibers, BFs possess excellent high-temperature resistance. These superior attributes indicate that BFs have potential for modifying CAC-based composite materials. Lu et al.[20] found that BFs have a very positive effect on the toughness and strength of polymer plates. In addition, Dias et al.[22] pointed out that BFs can effectively enhance the fracture toughness of geopolymer composites. Their research showed that the fracture toughness of fibers reinforce geopolymeric concretes (FRGC) with 0.5 and 1% BF increased by 14 and 111%, respectively, compared with that of cement materials. However, there was no mention of whether BFs have a similar effect on CAC at high temperatures. At the same time, the low polarity of the surface of BFs has a marked negative impact on its ability to be dispersed in the cement and its adhesion to the cement matrix. Therefore, suitable surface treatment protocols must be selected to improve the effects of modification. However, there are few reports on the surface treatment of BFs. Notably, low-temperature plasma treatment is a fast, environmentally friendly, and efficient treatment approach for surface modification of BFs.[23,24]

Therefore, BFs, as a new type of reinforcing material, are introduced into CAC-based composites in this study, and the properties of the BF-reinforced CAC composites are investigated at low temperature (50 °C) and high temperature (500 °C). In view of the problems related to the poor surface properties of BFs, low-temperature plasma is used herein to treat the BFs to improve their surface properties; this process is expected to further improve the modification effect. The effects of the temperature, effective fiber content, and curing age on the strength of CAC-based composites are discussed. This study is useful for the evaluation of fiber-reinforced CAC-based composites in cement structures that are used at high temperatures.

2. MATERIALS AND METHODS

2.1. Materials and Mix Proportions. This article uses the Chinese standard CAC, number A900, and uses slag as the auxiliary cementing material. The cement in the specimens was partially replaced with slag at a replacement ratio of 30% by weight.[25] The percentage slag was selected because the addition of about 30% blast furnace slag (BFS) has a positive effect on the pore size distribution of cement and can improve the thermal

https://doi.org/10.1021/acsomega.2c00617
ACS Omega 2023, 8, 1864−1875

Table 2. Chemical Properties of Cement and Slag (w/%)

oxides	CaO	SiO_2	Al_2O_3	MgO	SO_3	Fe_2O_3	Na_2O	K_2O	TiO_2	MnO
CAC	26.58	3.98	41.23	0.632	0.211	1.09	0.087	0.178	3.31	0.327
slag	36.5	31.16	11.97	9.12		0.796	0.574	0.039	2.61	0.469

conductivity and mechanical properties of the composite material under the action of high temperature. Further, the compressive strength of the sample is higher, and the microstructure of the sample at high temperature is more compact than that of the pure CAC sample. The chemical compositions of these materials are listed in Table 2. This article uses BF with high strength and toughness as the toughening material. The fibers have a very high tensile strength, which can reach 3−5 GPa. Moreover, research has found that the addition of BF at a ratio of 0−0.5% has a very positive effect on the performance of cement-based materials at high temperatures. Figure 2 shows the macroscopic image and microstructure of the BFs.

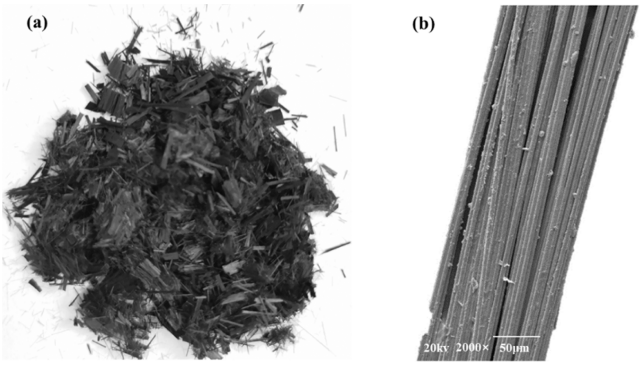

Figure 2. BF: (a) macrostructure image and (b) microstructure.

A laser particle size analyzer (Master Sizer 2000, Malvern UK) was used for particle size analysis of CAC and BFS, as shown in Figure 3. Table 3 shows the material properties of the BFs. Other materials, such as dispersants and fluid loss control agents that were used to optimize the slurry systems, were commercially obtained in China.

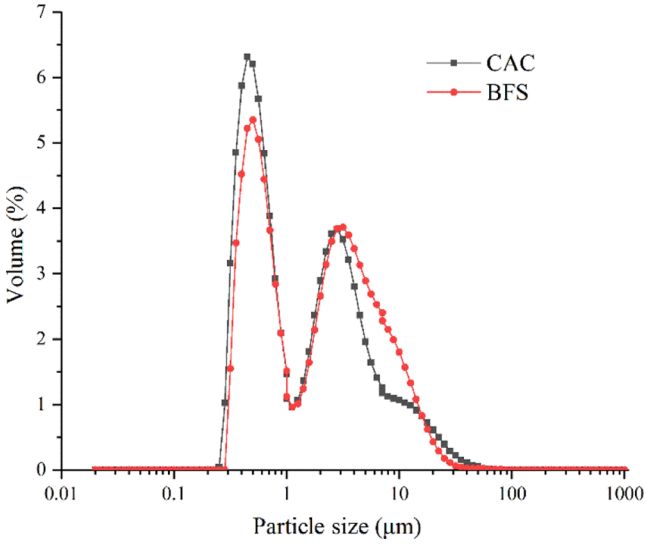

Figure 3. CAC and BFS particle size distribution.

2.2. Plasma Treatment. The principle of low-temperature plasma is to ionize and analyze air molecules into ions, electrons, and tiny particles and then use these tiny particles to continuously bombard the surface of the material to optimize the structure of the material surface. In this way, the hydrophilicity of the surface of the material is improved without causing damage to the surface of the material. The advantages of the low-temperature plasma technology are a simple process, convenient operation, low cost, no damage to materials, a fast processing speed, good treatment effects, low environmental pollution, and energy saving. It is currently widely used in the field of surface modification of materials.[26−29]

The surface of the BF was tailored by treatment for 90 s with low-temperature plasma at a power of 120 W using a plasma reactor (OPS DT-03) to improve the hydrophilicity and adhesion to the matrix.

2.3. Specimen Preparation. Cement, slag, and admixtures were mixed in the dry powder state and stirred uniformly, and then, BFs were added to the composite mixture at contents of 0, 0.1, 0.2, 0.3, 0.4, and 0.5% and then mixed with the required amount of water (W_{H_2O}/W_{binder} = 0.44/1 weight ratio) for 2 min. W_{H_2O}/W_{binder} = 0.44/1 weight ratio indicates that the required mass ratio of water to the compound mixture is 0.44, where the mixture was prepared according to the API RP-10B standard of the oil-well cement test method. The purpose of mixing for 2 min is to combine the compound mixture. The compound mixture is evenly mixed in the water while ensuring that the BF is evenly dispersed in the cement slurry. The cement slurry formula and slurry properties are shown in Tables 3 and 4.

According to Tables 3 and 4, the performance of the cement slurry is still relatively good after adding different amounts of BF. Slag has little effect on the setting time of CAC, and the thickening time of the cement slurry after adding the retarder is about 150 min, which meets the construction requirements.

The prepared cement slurry was poured into an experimental mold and cured at 50 °C and 100% relative humidity for a certain time. To explore the performance of these BF-reinforced cement-based composites at high temperatures, the hardened cement paste was placed in a water bath at 50 °C for 7 d. After 7 d of curing, the samples were dried at ambient temperature for 7 d and cured for 7 d in an electric heating furnace at 500 °C. The samples were heated from ambient temperature to 500 °C at a ramp rate of 5 °C/min. After reaching the designated age, the samples were cooled down in the furnace and then subjected to the relevant tests.

2.4. Curing Age and Conditions. The curing age and conditions for all the hardened cement paste samples used in this experiment are summarized in Table 6.

2.5. Test Setup and Instrumentation. According to the ASTM C109 standard, the compressive strength test was performed on samples with dimensions of 50.8 mm × 50.8 mm × 50.8 mm at 1, 3, 7,1 4, 21, and 28 d of aging. According to the Chinese National Standard 3904 (CNS 3904), the cement sample was poured into a cylindrical mold (24.5 × 50.8 mm^2), and the tensile strength of the cement sample was tested using an electro-hydraulic testing machine according to the Brazilian

https://doi.org/10.1021/acsomega.2c00617
ACS Omega 2023, 8, 1864−1875

Table 3. Formulations of the Cement Slurry (% by Mass of CAC)[a]

ID	cement/%	BF/%	slag/%	PS/%	G33S/%	USZ/%	XP-1/%	water/%	density/(g cm^{-3})
1	100	0	30	0.5	0.5	0.2	0.2	44	1.85
2	100	0.1	30	0.5	0.5	0.2	0.2	44	1.85
3	100	0.2	30	0.5	1.0	0.5	0.2	44	1.85
4	100	0.3	30	0.6	1.0	0.5	0.2	44	1.85
5	100	0.4	30	0.6	1.5	0.8	0.2	44	1.85
6	100	0.5	30	0.6	1.5	0.8	0.2	44	1.85

[a]Note: PS: retarder; G33S: fluid loss agent; USZ: dispersant; XP-1: defoamer.

Table 4. Conventional Properties of Different Cement Slurries

					stability Δρsc/%		
ID	rheology index (n)	consistency coefficients (k)/Pa s	static fluid loss/mL	thickening time/min	top	middle	bottom
1	0.96	0.34	22	156	100.0	100.0	100.0
2	0.94	0.37	22	151	100.0	100.0	100.0
3	0.90	0.40	21	162	100.0	100.0	100.0
4	0.88	0.42	21	153	99.9	100.0	100.1
5	0.88	0.43	21	155	99.9	100.0	100.1
6	0.80	0.54	20	145	99.7	100.2	100.5

Table 5. Parameters Related to BFs

fiber type	length (mm)	tensile strength (GPa)	thermostable temperature (°C)
basalt fibres	~5	3−5	650

splitting test method.[30] The triaxial compression test was performed on the samples using a Triaxial Rock Mechanics test system (RTR-1000, GCTS Co., USA). The confining pressure of 20.4 MPa was selected in line with rock triaxial mechanics tests in most current studies.[31,32] The test was also carried out according to the standard SL237-017-1999.

An X-ray photoelectron spectroscopy (XPS) spectrometer (Kratos, AXIS Supra) was used to analyze the untreated and oxygen plasma-treated BFs.

The sample microstructure was investigated using scanning electron microscopy (SEM, QUANTA 450). Atomic force microscopy (AFM) images were obtained using a Bruker SPM8 AFM scanning probe microscope. For AFM analysis, the BFs were attached to a silicon wafer. Because plasma treatment has strong time lines, the relevant manufacturing of cement should be performed immediately after the BF is plasma-treated.

3. RESULTS AND DISCUSSION

3.1. Morphological Analysis of Basalt Fibers by AFM.

The SEM images and AFM images of the original BFs and plasma-treated BFs are presented in Figures 4 and 5, respectively. The average roughness is summarized shown in Table 7. AFM analysis was conducted over a 400 × 400 nm area on the fiber surface.

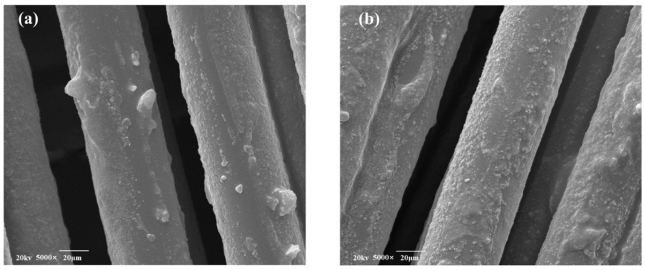

Figure 4. SEM topographical images of the BFs: (a) untreated and (b) plasma-treated.

The untreated BFs (Figure 5a,c) had a relatively smooth surface with an average surface roughness of 59.2 nm, while the plasma-treated fibers (Figure 5b,d) exhibited a higher roughness

Table 6. Hardened Cement Paste Curing Age and Conditions

curing age		curing conditions	purpose
sample with curing age ≤14 d	1d	50 °C × 20.4 MPa	simulating curing conditions at downhole before in situ combustion
	3d	50 °C × 20.4 MPa	
	7d	50 °C × 20.4 MPa	
	14d	50 °C × 20.4 MPa	
sample with the curing age at 21 d		high temperature (500 °C): cured at 50 °C × 20.4 MPa for 14 d and then at 500 °C × 0.1 MPa for 7 d	simulating curing conditions at downhole and in situ combustion conditions
		low temperature (50 °C): cured for 21 d at 50 °C × 20.4 MPa	control sample: in control with sample curing at 500 °C, investigating the effect of high temperature on hardened cement paste
sample with the curing age at 28 d		high temperature (500 °C): cured at 50 °C × 20.4 MPa for 14 d and then at 500 °C × 0.1 MPa for 14 d	simulating curing conditions at downhole and in situ combustion conditions
		low temperature (50 °C): cured for 28 d at 50 °C × 20.4 MPa	control sample: in control with sample curing at 500 °C, investigating the effect of high temperature on hardened cement paste

https://doi.org/10.1021/acsomega.2c00617
ACS Omega 2023, 8, 1864−1875

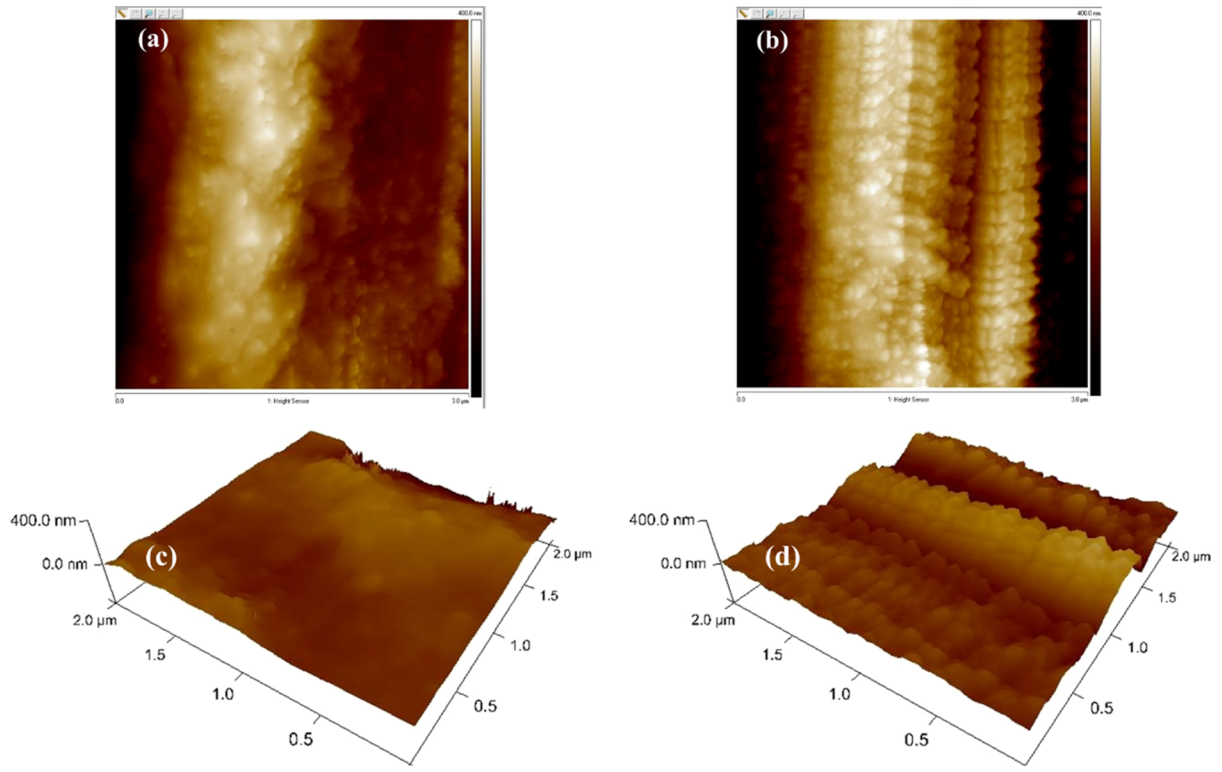

Figure 5. AFM topographical images of the BFs: (a,c) untreated and (b,d) plasma-treated.

Table 7. Surface Roughness of Untreated and Plasma-Treated BFs

sample	untreated	Plasma-treated
RMS (nm)	59.2	96.9

of approximately 96.9 nm, indicating that the aggressive nature of the plasma treatment resulted in non-homogeneous distribution of affected areas on the fiber surface.

3.2. XPS Analysis. The XPS results for the control and plasma-treated fibers are shown in Figure 6. The composition determined using XPS was remarkably similar for both sizing conditions. C 1s, O 1s, Si 2p, and N 1s core lines were detected in the XPS profiles.[21] Analysis of the BFs before and after plasma modification showed a significant difference between the silicon and nitrogen contents of the two types of fibers. This is because the surface of the BF contained more silicon and oxygen after plasma treatment.

The XPS data for the coated fibers were calibrated against the binding energy peak at 285 eV, which corresponds to the C−C bond.[22] Deconvolution of the C 1s peak resulted in three peaks (Figure 7): C−C (284.7 eV), C−O (286 eV), and O−C═O (289 eV).[22] The plasma-treated BFs had more polar functional groups on the fiber surface, which improved the wettability of the fiber, in turn enhancing the adhesion of the fibers to the cement composites.[19]

3.3. Mechanical Properties. *3.3.1. Strength.* The tensile and compressive strengths of the samples treated at 50 °C with

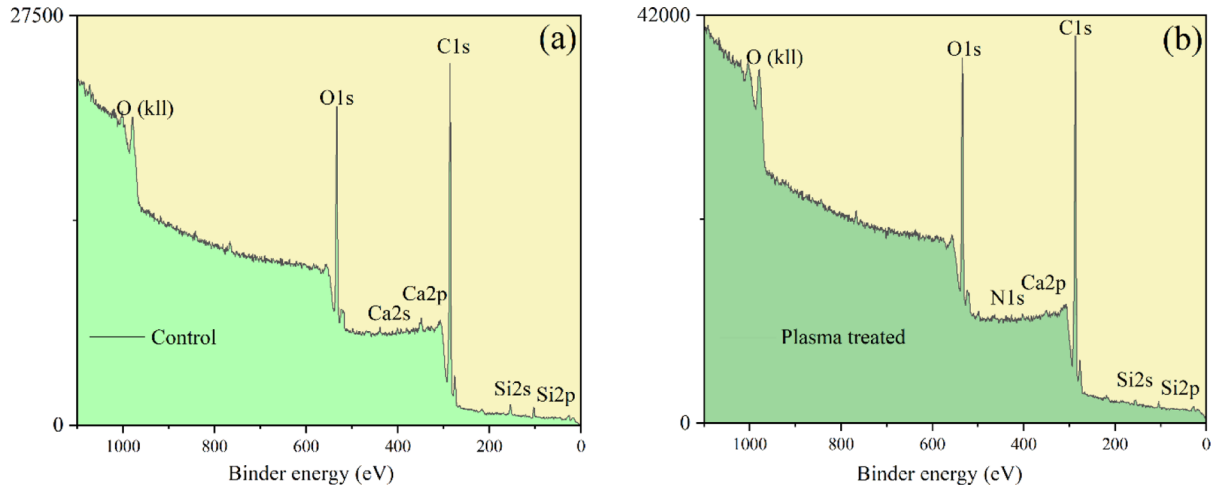

Figure 6. XPS survey spectra of BF: (a) control and (b) plasma-treated.

https://doi.org/10.1021/acsomega.2c00617
ACS Omega 2023, 8, 1864−1875

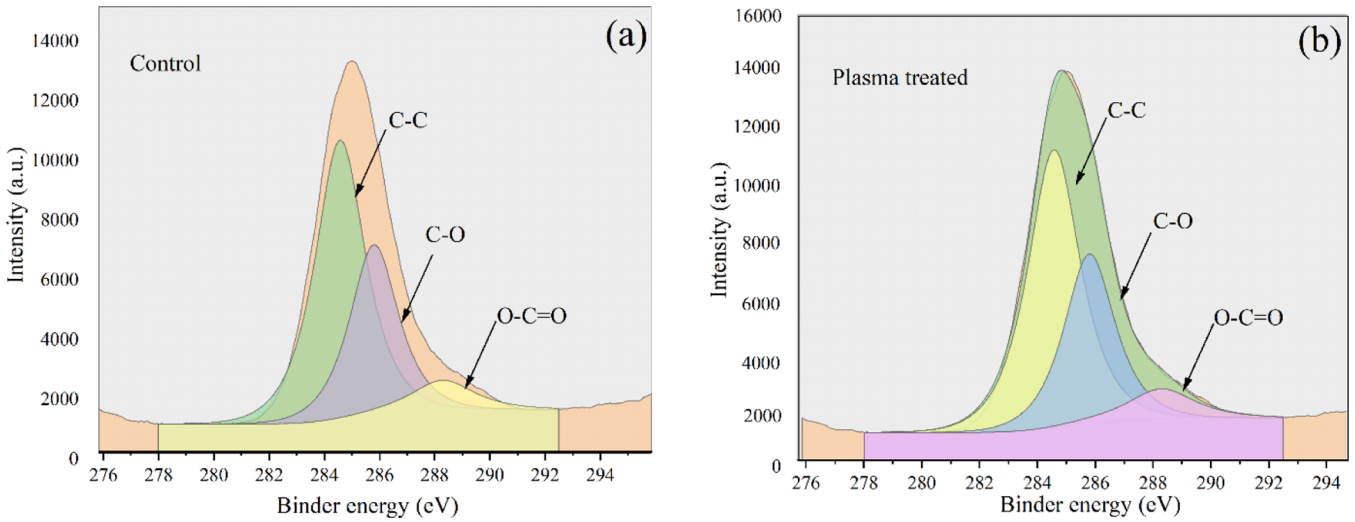

Figure 7. High-resolution C 1s XPS scan for BF: (a) control and (b) plasma-treated.

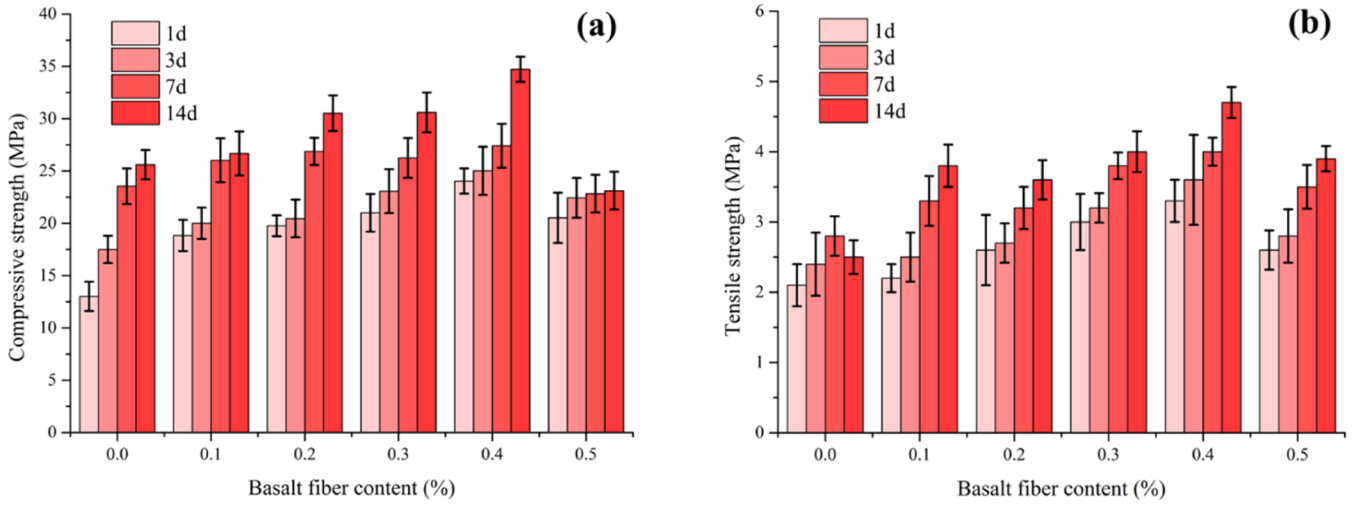

Figure 8. Compressive strength (a) and tensile strength (b) of plain cement sample and fibre-reinforced cement samples cured at 50 °C for 1, 3, 7, and 14 d.

increasing curing age are illustrated in Figure 8. For the samples aged for different times, the experimental results show that the tensile strengths and compressive strengths increased gradually with higher BF content. However, the experimental results show that when the amount of BF reached 0.4−0.5%, the strength of the cement-based material was lower than the maximum strength. Moreover, the strength of the cement with BFs was significantly improved compared to that of the control. When the BF content in the cement was 0.4%, the compressive strength and tensile strength increased from 25.6 to 34.72 MPa and from 3.72 to 4.70 MPa, reaching the maximum values, corresponding to increases of 35.6 and 26.34%, respectively; these values are greater than those of the control-cement samples at 14 d. These findings indicate the superior reinforcement capacity of the BFs, which is mainly due to the excellent mechanical properties of the fibers, as previously stated by Lu.[20,33] The increase in the mechanical strength also demonstrates strong bonding between the cement matrix and the fibers. In contrast, the improved mechanical strength could also be partly explained by the satisfactory compatibility between the fiber and the cement. These results highlight the potential of BFs as a reinforcing agent in the cement matrix. When fiber-reinforced cement samples are subjected to simultaneous exposure to mechanical and environmental stresses, the BFs accommodate some of the force on part of the cement matrix, leading to an overall enhancement of the mechanical properties. The BFs also bear stress during fracture growth. This can be attributed to the BFs, as reinforcing materials, compensating for the decrease in the mechanical strength in response to a load. Additionally, the increase in the strength of the fiber-reinforced cement may be due to the increase in the amount of energy absorbed at failure.[34] Many previous studies have pointed out that the addition of fibers or whiskers can enhance the energy absorption efficiency of cement, which is mainly due to the bridging effect of the fibers and whiskers in the matrix.[7,35,36]

The compressive strength and tensile strength of the hardened cement paste after curing for 21 and 28 d according to the simulated curing conditions shown in Table 5 are shown in Figure 8. The tensile strength and compressive strength of the cement cured for 7 d at 50 °C and dried at ambient temperature for 7 d as well as the sample cured for 7 d at 500 °C are shown in Figure 9. The experimental results show that increasing the loading of the BFs initially increased the tensile and compressive

https://doi.org/10.1021/acsomega.2c00617
ACS Omega 2023, 8, 1864−1875

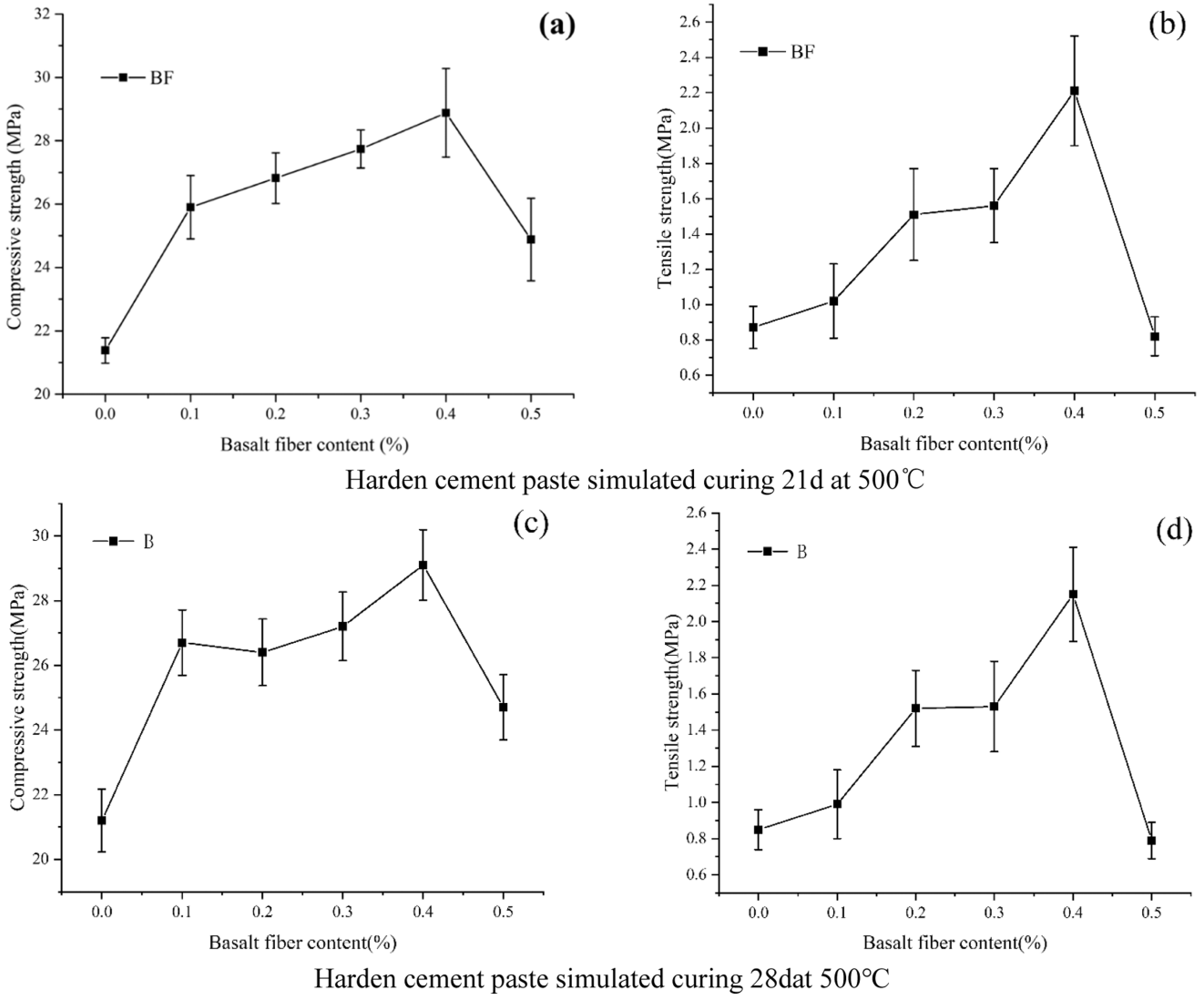

Figure 9. Compressive strength (a,c) and tensile strength (b,d) of the samples.

strengths of the cement-based materials, followed by a decrease; the optimal fiber loading was 0.4%. Compared with the control sample, the fiber addition increased the compressive strength and tensile strength. After curing for 21 d, the compressive strength and tensile strength of hardened cement paste added with 0.4% BF increased from 21.38 to 28.88 MPa and 0.88 to 2.21 MPa, respectively; compared with the control group, the increase was approximately 35.1 and 151.1%, respectively. After curing for 28 d, the compressive strength and tensile strength of hardened cement paste with 0.4% BF added were increased from 21.20 to 29.11 MPa and from 0.85 to 2.15 MPa, respectively; compared with the control group, the increase was approximately 37.3 and 152.9%, respectively. Incorporating the optimal amount of BFs can effectively increase the toughness of the cement matrix, as determined by reduction of the chemical bond of the fiber/matrix interface.[37] Additionally, the flexible structure of the BFs can increase the interface roughness between the fiber and the cement, which increases the frictional bonding strength and thus the tensile strain capacity.

Figure 10 shows the effect of the plasma-modified 0.4% BFs on the tensile and compressive strengths of the CAC-based composites at low (50 °C) and high (500 °C) temperatures. The plasma-modified BFs exerted an improved toughening effect on the cement samples to some extent. The initial tensile strength and compressive strength of the samples cured at 50 °C for 21 d were 34.72 and 4.72 MPa, respectively, and increased to 40.7 and 5.07 MPa, representing increases of 17.2 and 7.4%, respectively. At the same time, the initial tensile strength and compressive strength of the samples cured at 50 °C for 28 d were 34.11 and 4.55 MPa, respectively, and increased to 41.15 and 5.21 MPa, representing increases of 20.6 and 14.5%, respectively. This reflects that the toughening effect of the BFs can be significantly improved by plasma treatment.

It can also be seen from the figure that when the hardened cement paste is cured for 21 d, the high-temperature compressive strength and tensile strength increased from 28.88 and 1.55 to 35.23 and 1.87 MPa, respectively, an increase of 21.98 and 20.6%. At the same time, when the hardened cement paste is cured for 28 d, the high-temperature compressive strength and tensile strength increased from 28.26 and 1.5 to 29.1 and 2.15 MPa, respectively, an increase of 3.0 and 43.3%, respectively. In addition, the plasma surface-modified BFs still had good toughening and strengthening effects on CAC at 500 °C.

3.3.2. Stress−Strain. The stress−strain relationship for cement-based materials with and without BFs has been

https://doi.org/10.1021/acsomega.2c00617
ACS Omega 2023, 8, 1864−1875

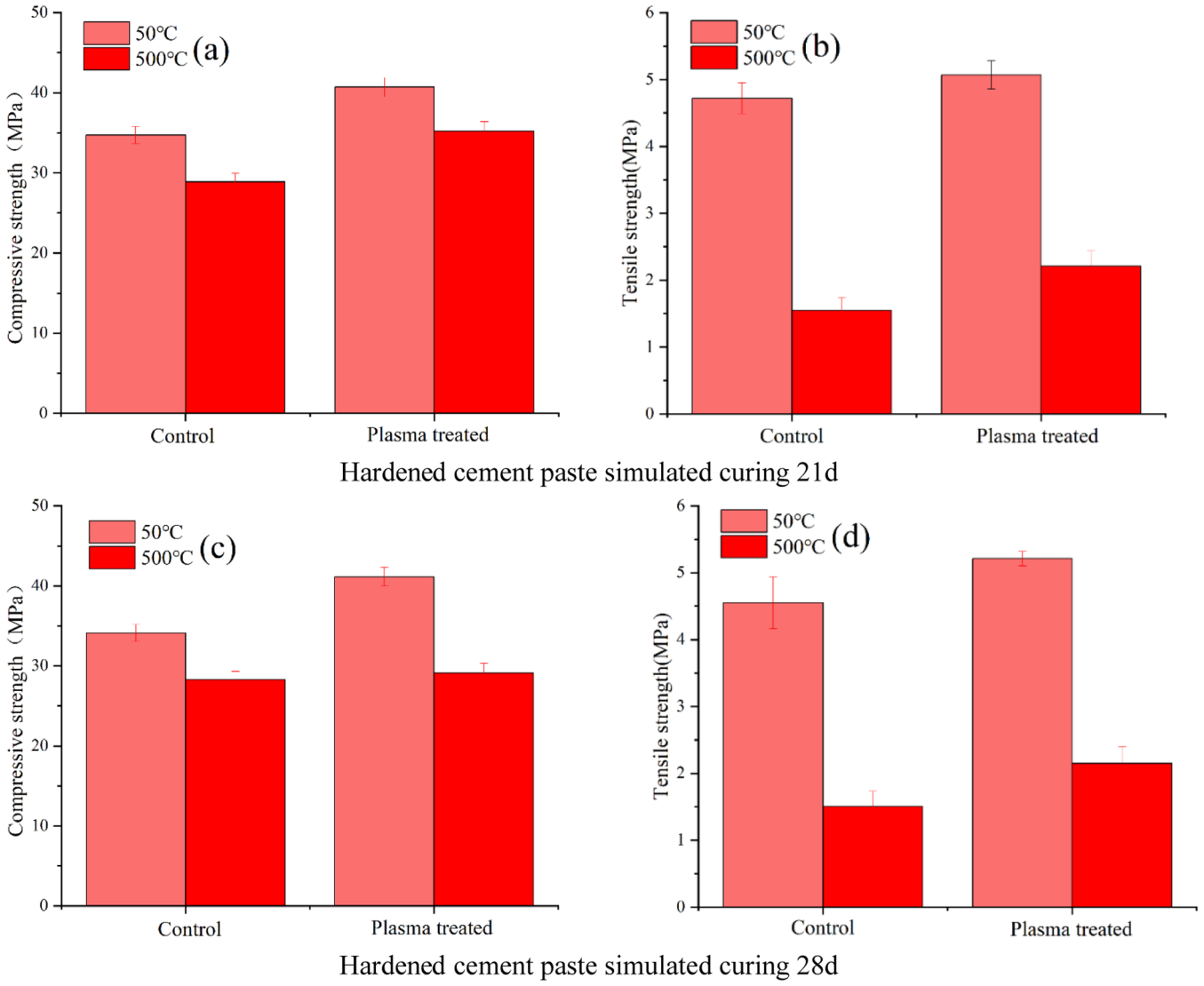

Figure 10. Compressive strength (a,c) and tensile strength (b,d) of CAC-based composites with 0.4% BFs.

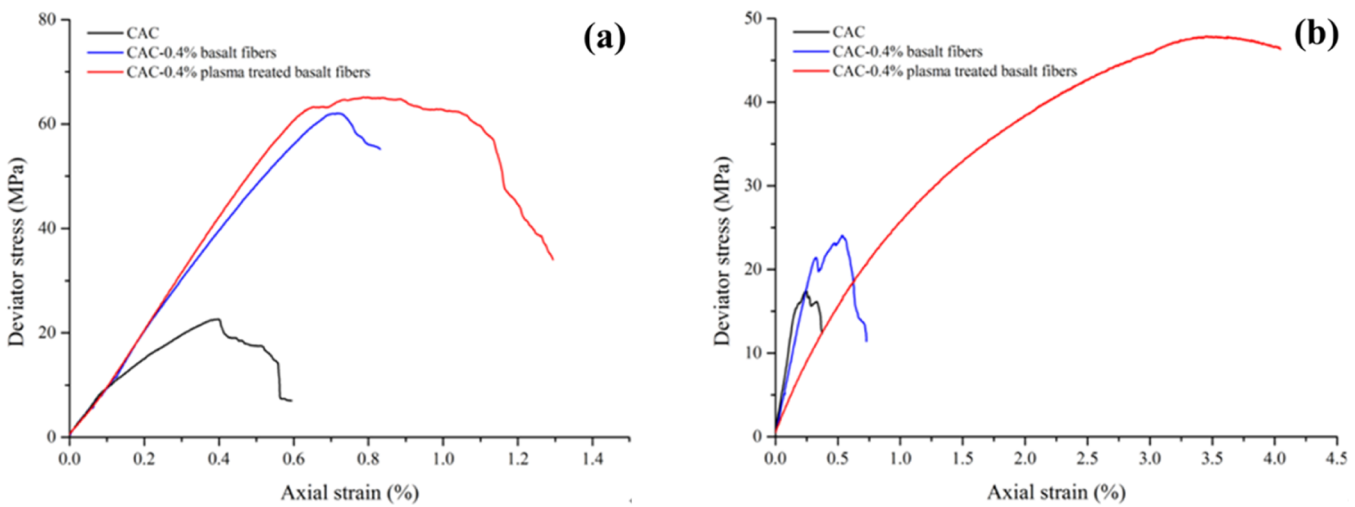

Figure 11. Stress−strain curves of the control samples and samples with 0.4% BFs [(a) cured at 50 °C and (b) cured at 500 °C].

studied.[33] However, the effects of fibers on the performance of CAC at 500 °C are still poorly studied. The triaxial stress−strain curves for the cement with 0.4% BFs and that with no added fibers at different temperatures are shown in Figure 11. The addition of 0.4% BF led to a much higher peak in the stress−strain curve than that of the control. The plasma-treated BF-

https://doi.org/10.1021/acsomega.2c00617
ACS Omega 2023, 8, 1864−1875

reinforced CAC-based composites presented superior stress−strain capacity, reflecting greater toughness than the untreated fiber-reinforced cement and plain cement samples.

The peak stress of the cement substrate may be affected to some extent by the lower interface strength between the fiber and the cement matrix.[38−40] However, compared with the cement samples without BFs, the peak stress was higher for the cement samples with BFs, as shown in Table 8. After a high

Table 8. Mechanical Properties of CAC-Based Composites (500 °C)

samples	dynamic elastic modulus (MPa)	Poisson ratio	peak stress (MPa)
control samples	9932.0	0.278	17.4
untreated BF	8547.1	0.201	24.1
Plasma-treated BF	2886.0	0.172	47.9

temperature of 500 °C, adding 0.4% BFs can effectively improve the toughness of CAC composites in high-temperature environments. At the same time, it can be seen from Table 8 that the addition of plasma-treated BFs can greatly reduce the Poisson's ratio of elastic modulus of CAC composites, thereby improving the toughness of CAC composites to a certain extent. This indicates excellent adhesion between the BFs and cement matrix at a high temperature (500 °C) and that the addition of 0.4% BFs is effective for improving the toughness of CAC in high-temperature environments. This is mainly due to the bridging effect of the fibes. When the cement matrix is stressed, part of the stress is transferred to the fiber, which resists cracking of the cement matrix to a certain extent.[35] Meanwhile, the BFs have a much higher tensile modulus and strength than the cement matrix. Consequently, the uniform dispersion and anisotropic orientation of the fibers can reinforce the mechanical properties of the cement composites.[41] Hence, increasing the fiber fraction to a particular amount increases both the strength and toughness of the cement.

3.4. SEM Analysis. As shown in Figure 12, the microstructure of the samples was observed by SEM to investigate the distribution of the fibers in the cement matrix and the mechanism of reinforcement by the BFs. The microstructure of the BF-modified CAC without plasma treatment is shown in Figure 12a−c. When a force acts on the fiber in the cement matrix, the force is deflected by cracking of the matrix and the fiber is broken, thereby enhancing the mechanical properties of the cement. When the cement is subjected to external stress, cracks are generated inside the cement, and the cracks expand. When the BF is toughened using plasma, the BF has a higher strength and consumes the fracture energy of the cement. This causes deflected crack propagation in the sample. At the same time, when the fiber is present in the cement matrix, it can connect the cement matrix on both sides of the crack and increase the resistance of the hardened cement paste to external stress. Furthermore, when the hardened cement paste is subjected to an external force that causes internal cracks, the cracks pass through the high-strength and high-toughness fibers inside the cement, which consume part of the fracture energy, thereby effectively suppressing crack propagation and reinforcing the cement composite.

The microstructure of the BF-toughened aluminate cement after plasma modification is shown in Figure 12d−f. Good interfacial bonding resulting from the modified BF in the cement matrix can better combine with cement hydration products.

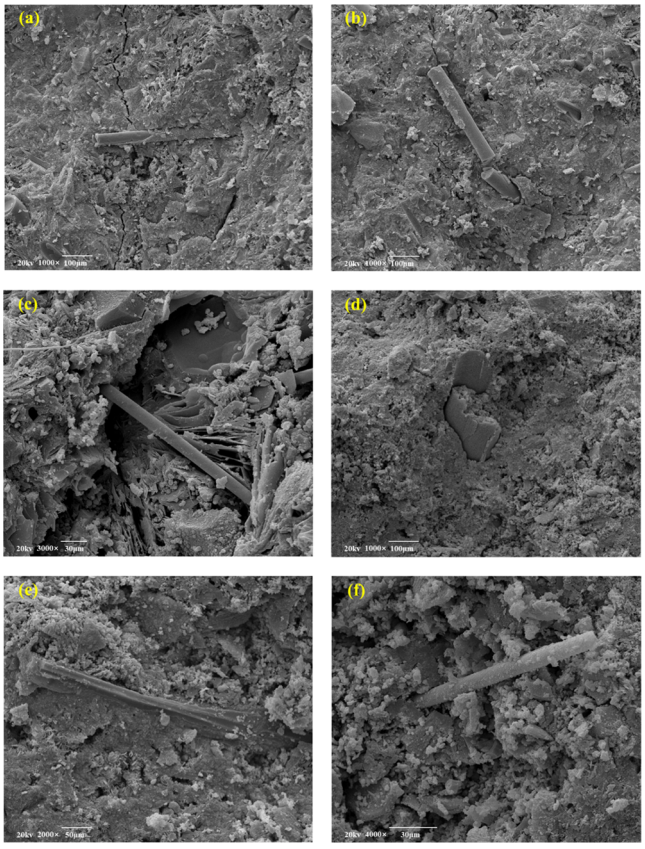

Figure 12. SEM image of cement composites: (a−c) untreated and (d−f) plasma-treated.

Compared with the unmodified BFs, the modified BFs had a rougher surface structure, the surface contains more polar functional groups, and these functional groups can produce a good combination with cement hydration products; thus, the latter undergo better interfacial bonding with the cement matrix. When cracks are generated by external stress, the cracks form in the interfacial transition zone between the BF and the cement matrix, and the cement matrix in the interfacial transition zone has a denser structure and higher strength compared to the untreated BF-reinforced CAC-based composites. Therefore, plasma treatment of the surface structure of the BF confers superior mechanical properties and enhanced toughness to the samples.

Studies have shown that certain types of fiber/matrix interactions can increase the energy absorption of reinforced cement composites. These include multiple effects, such as interfacial adhesion related to random fiber orientation.[42,43] Weak interfacial bonding would cause the fiber to be pulled out of the matrix, as presented in Figure 13, and consequently deteriorate the mechanical properties. On the other hand, a too strong interface can cause the fibers to break because they cannot be stretched.[43]

4. CONCLUSIONS

The properties of plasma-modified BF-reinforced CAC slag-based composites and the toughening mechanism were investigated. The following conclusions were drawn from the results.

(1) The BFs afforded a good toughening and strengthening effect at high temperatures. With 0.4% BF addition, the

https://doi.org/10.1021/acsomega.2c00617
ACS Omega 2023, 8, 1864−1875

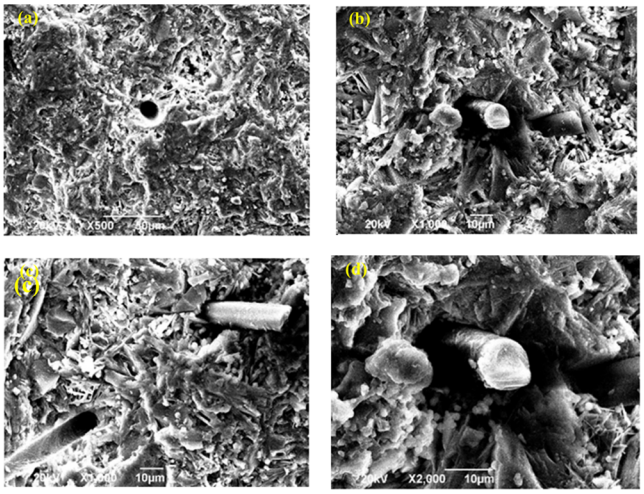

Figure 13. SEM micrograph of CAC-based composites showing pull-out of BFs (a–d).

high-temperature compressive and tensile strength respectively increased from 21.38 and 0.88 to 28.88 and 1.63 MPa, respectively, where the strength increased by 35.08 and 74.7%, respectively, when compared with those of the control samples. When the hardened cement paste is cured by simulated curing for 21 d, plasma modification of the BFs resulted in a better reinforcing effect, and the high-temperature compression and tensile strength of the samples increased from 28.88 and 1.52 to 35.23 and 1.87 MPa, respectively, an increase of 21.98 and 20.6%, respectively, compared with the untreated BFs. When the hardened cement paste is cured by simulated curing for 28 d, the high-temperature compressive strength and tensile strength with plasma modification increased from 28.26 and 1.5 to 29.1 and 2.15 MPa, respectively, an increase of 3.0 and 43.3%, respectively.

(2) When the BF-reinforced CAC slag-based composites were subjected to an external force that caused internal cracking, within the crack, part of the fracture energy was consumed by the higher-strength and higher-toughness fibers inside the cement matrix. Therefore, BFs can effectively suppress the propagation of cracks and enhance the toughness of CAC slag-based composites.

(3) Debonding and pull-out of the BFs are the main toughening mechanisms in CAC slag-based cement composites, as confirmed by microstructural analysis.

AUTHOR INFORMATION

Corresponding Author

Jintang Guo − *School of Chemical Engineering and Technology, Tianjin University, Tianjin 300350, P. R. China*; Email: jtguo@tju.edu.cn

Authors

Hua Zhang − *School of Chemical Engineering and Technology, Tianjin University, Tianjin 300350, P. R. China*

Xiaowei Cheng − *School of New Energy and Materials, Southwest Petroleum University, Chengdu 610500, China; State Key Laboratory of Oil and Gas Reservoir Geology and Exploitation, Southwest Petroleum University, Chengdu 610500, China*; orcid.org/0000-0002-7975-7254

Jingxuan Cai − *School of New Energy and Materials, Southwest Petroleum University, Chengdu 610500, China; State Key Laboratory of Oil and Gas Reservoir Geology and Exploitation, Southwest Petroleum University, Chengdu 610500, China*

Xiucheng Ni − *School of New Energy and Materials, Southwest Petroleum University, Chengdu 610500, China; State Key Laboratory of Oil and Gas Reservoir Geology and Exploitation, Southwest Petroleum University, Chengdu 610500, China*

Complete contact information is available at: https://pubs.acs.org/10.1021/acsomega.2c00617

Notes

The authors declare no competing financial interest.

ACKNOWLEDGMENTS

The authors are grateful for the support provided from the Major engineering technology field test project of CNPC "Field Test of Cementing Seal Integrity Technology in Complex Ultra-Deep Wells" (2020F-49). The authors also would like to thank Advanced Cementing Materials Research Center of SWPU for the kind assistance in laboratory testing.

ABBREVIATIONS

CAC, calcium aluminate cement
ISC, in situ combustion
BFS, blast furnace slag
BF, basalt fiber
d, day
XPS, X-ray photoelectron spectroscopy
AFM, atomic force microscopy
SEM, scanning electron microscopy
RMS, mean surface roughness
C 1s, by measuring the binding energy of 1s electrons, the chemical element "carbon" can be identified from the XPS spectrum, which is professionally recorded as C 1s
O 1s, by measuring the binding energy of 1s electrons, the chemical element "oxygen" can be identified from the XPS spectrum, which is professionally recorded as O 1s
Si 2p, by measuring the binding energy of 2p electrons, the chemical element "silicon" can be identified from the XPS spectrum, which is professionally recorded as Si 2p
N 1s, by measuring the binding energy of 1s electrons, the chemical element "nitrogen" can be identified from the XPS spectrum, which is professionally recorded as N 1s
C−C, carbon−carbon single bond
C−O, carbon-oxygen single bond
O−C═O, carboxyl

REFERENCES

(1) Abo-El-Enein, S. A.; El-Gamal, S. M. A.; Aiad, I. A.; Azab, M. M.; Mohamed, O. A. Early hydration characteristics of oil well cement pastes admixed with newly prepared organic admixture. *HBRC J.* **2018**, *14*, 207−214.

(2) Wang, C.; Meng, R.; Xiao, F.; Wang, R. Synthesis and performance evaluation of a novel biodegradable dispersant for offshore cementing. *J. Nat. Gas Sci. Eng.* **2017**, *38*, 582−589.

(3) Cheng, X.; Qin, D.; Chen, Z.; Pu, Y.; Han, Z.; Li, D.; Gao, X.; Wang, J.; Zhang, C.; Liu, K. Mechanical response and crack propagation of oil well cement under dynamic and static loads. *J. Adhes. Sci. Technol.* **2019**, *33*, 1658−1675.

(4) Suyan, K. M.; Dasgupta, D.; Garg, S. P.; Jain, V. K. Novel cement composition for completion of thermal recovery (ISC) wellbores. *SPE/IADC INDIAN Drilling Technology Conference and Exhibition*; OnePetro, 2006; pp 73−78.
(5) Mac, F.; Diego, O.; Hollman, N.; Energy, P. R.; Javier, U.; Alberto, G. Long-Term Calcium Phosphate Cement for In-Situ Combustion Project Synchronized Thermal Additional Recovery (STAR) Project. *SPE Heavy Oil Conference*; OnePetro, 2014; pp 1−10.
(6) Moore, R. G.; Belgrave, J. D. M.; Ursenbach, M. G.; Laureshen, C. J.; Mehta, S. A.; Gomez, P. A.; Jha, K. N. In situ combustion performance in steam flooded heavy oil cores. *J. Can. Pet. Technol.* **1999**, *38*, 50.
(7) Cheng, X.; Dong, Q.; Li, Z.; Guo, X. High-temperature mechanical properties of calcium sulfate whisker-reinforced high-alumina cement. *Mag. Concr. Res.* **2020**, *72*, 55−67.
(8) Xu, Y.; Xu, Q.; Chen, S.; Li, X. Self-restraint thermal stress in early-age concrete samples and its evaluation. *Constr. Build. Mater.* **2017**, *134*, 104−115.
(9) Lee, N. K.; Koh, K. T.; Park, S. H.; Ryu, G. S. Microstructural investigation of calcium aluminate cement-based ultra-high performance concrete (UHPC) exposed to high temperatures. *Cem. Concr. Res.* **2017**, *102*, 109−118.
(10) Shoukry, H.; Kotkata, M. F.; Abo-EL-Enein, S. A.; Morsy, M. S.; Shebl, S. S. Thermo-physical properties of nanostructured lightweight fibre reinforced cementitious composites. *Constr. Build. Mater.* **2016**, *102*, 167−174.
(11) Tonoli, G. H. D.; Savastano, H.; Santos, S. F.; Dias, C. M. R.; John, V. M.; Lahr, F. a. R. Hybrid Reinforcement of Sisal and Polypropylene Fibres in Cement-Based Composites. *J. Mater. Civ. Eng.* **2011**, *23*, 177−187.
(12) Silva, F. d. A.; Mobasher, B.; Filho, R. D. T.; Filho, T.; Silva, F. de A.; Mobasher, B.; Filho, R. D. T. Cracking mechanisms in durable sisal fibre reinforced cement composites. *Cem. Concr. Compos.* **2009**, *31*, 721−730.
(13) Hwang, C.-L.; Tran, V.-A.; Hong, J.-W.; Hsieh, Y.-C. Effects of short coconut fibre on the mechanical properties, plastic cracking behavior, and impact resistance of cementitious composites. *Constr. Build. Mater.* **2016**, *127*, 984−992.
(14) Garcés, P.; Zornoza, E.; Alcocel, E. G.; Galao, Ó.; Andión, L. G. Mechanical properties and corrosion of CAC mortars with carbon fibres. *Constr. Build. Mater.* **2012**, *34*, 91−96.
(15) Niu, D.; Jiang, L.; Bai, M.; Miao, Y. Study of the performance of steel fibre reinforced concrete to water and salt freezing condition. *Mater. Des.* **2013**, *44*, 267−273.
(16) Kim, B.-J.; Yi, C.; Ahn, Y.-r. Effect of embedment length on pullout behavior of amorphous steel fibre in Portland cement composites. *Constr. Build. Mater.* **2017**, *143*, 83−91.
(17) Canal, C.; Gallinetti, S.; Ginebra, M.-P. Low-Pressure Plasma Treatment of Polylactide Fibres for Enhanced Mechanical Performance of Fibre-Reinforced Calcium Phosphate Cements. *Plasma Processes Polym.* **2014**, *11*, 694−703.
(18) Trejbal, J. Mechanical properties of lime-based mortars reinforced with plasma treated glass fibres. *Constr. Build. Mater.* **2018**, *190*, 929−938.
(19) Gallinetti, S.; Mestres, G.; Canal, C.; Persson, C.; Ginebra, M.-P. A novel strategy to enhance interfacial adhesion in fi ber-reinforced calcium phosphate cement. *J. Mech. Behav. Biomed. Mater.* **2017**, *75*, 495−503.
(20) Lu, Z.; Xian, G.; Li, H. Effects of elevated temperatures on the mechanical properties of basalt fibres and BFRP plates. *Constr. Build. Mater.* **2016**, *127*, 1029−1036.
(21) Wei, B.; Cao, H.; Song, S. Tensile behavior contrast of basalt and glass fibres after chemical treatment. *Mater. Des.* **2010**, *31*, 4244−4250.
(22) Dias, D. P.; Thaumaturgo, C. Fracture toughness of geopolymeric concretes reinforced with basalt fibres. *Cem. Concr. Compos.* **2005**, *27*, 49−54.
(23) Zhang, C.; Li, Y.; Cheng, X.; Liang, S.; Guo, X.; Zhao, H.; Song, Y. Effects of plasma-treated rock asphalt on the mechanical properties and microstructure of oil-well cement. *Constr. Build. Mater.* **2018**, *186*, 163−173.
(24) Zhang, C.; Cai, J.; Cheng, X.; Zhang, X.; Guo, X.; Li, Y. Interface and crack propagation of cement-based composites with sulfonated asphalt and plasma-treated rock asphalt. *Constr. Build. Mater.* **2020**, *242*, 118161.
(25) Cheng, X.; Dong, Q.; Ma, Y.; Zhang, C.; Gao, X.; Yu, Y.; Wen, Z.; Zhang, C.; Guo, X. Mechanical and thermal properties of aluminate cement paste with blast furnace slag at high temperatures. *Constr. Build. Mater.* **2019**, *228*, 116747.
(26) Gao, L.; Shi, X.; Wu, X. Applications and challenges of low temperature plasma in pharmaceutical field. *J. Pharm. Anal.* **2021**, *11*, 28−36.
(27) Sanito, R. C.; You, S.-J.; Wang, Y.-F. Degradation of contaminants in plasma technology: An overview. *J. Hazard. Mater.* **2022**, *424*, 127390.
(28) Duarte, S.; Panariello, B. H. D. Comprehensive biomedical applications of low temperature plasmas. *Arch. Biochem. Biophys.* **2020**, *693*, 108560.
(29) Redmer, R. Physical properties of dense, low-temperature plasmas. *Phys. Rep.* **1997**, *282*, 35−157.
(30) Zhang, C.; Song, Y.; Wang, W.; Guo, X.; Li, H. The influence of sulfonated asphalt on the mechanical properties and microstructure of oil well cement paste. *Constr. Build. Mater.* **2017**, *132*, 438−445.
(31) Sarasini, F.; Tirillò, J.; Sergi, C.; Carolina, M. C.; Seghini, L.; Graupner, N. Eff ect of basalt fi bre hybridisation and sizing removal on mechanical and thermal properties of hemp fi bre reinforced HDPE composites. *Compos. Struct.* **2018**, *188*, 394−406.
(32) Trejbal, J.; Nežerka, V.; Somr, M.; Fládr, J.; Potocký, Š.; Artemenko, A.; Tesárek, P. Deterioration of bonding capacity of plasma-treated polymer fi ber reinforcement. *Cem. Concr. Compos.* **2018**, *89*, 205−215.
(33) Cao, M.; Zhang, C.; Lv, H.; Xu, L. Characterization of mechanical behavior and mechanism of calcium carbonate whisker-reinforced cement mortar. *Constr. Build. Mater.* **2014**, *66*, 89−97.
(34) Al-tulaian, B. S.; Al-shannag, M. J.; Al-hozaimy, A. R. Recycled plastic waste fibres for reinforcing Portland cement mortar. *Constr. Build. Mater.* **2016**, *127*, 102−110.
(35) Kheradmand, M.; Mastali, M.; Abdollahnejad, Z.; Pacheco-Torgal, F. Experimental and numerical investigations on the flexural performance of geopolymers reinforced with short hybrid polymeric fibres. *Composites, Part B* **2017**, *126*, 108−118.
(36) Chakraborty, S.; Kundu, S. P.; Roy, A.; Adhikari, B.; Majumder, S. B. Polymer modified jute fibre as reinforcing agent controlling the physical and mechanical characteristics of cement mortar. *Constr. Build. Mater.* **2013**, *49*, 214−222.
(37) Ma, H.; Cai, J.; Lin, Z.; Qian, S.; Li, V. C. CaCO3whisker modified Engineered Cementitious Composite with local ingredients. *Constr. Build. Mater.* **2017**, *151*, 1−8.
(38) Huang, S.; Cheng, X.; Guo, X.; Shi, Y.; Wang, W. Ethanol plasma-induced polymerization of carbon fibre surface for improving mechanical properties of carbon fibre-reinforced lightweight oil well cement. *Appl. Surf. Sci.* **2019**, *497*, 143765.
(39) Xiaowei, C.; Sheng, H.; Xiaoyang, G.; Wenhui, D. Crumb waste tire rubber surface modification by plasma polymerization of ethanol and its application on oil-well cement. *Appl. Surf. Sci.* **2017**, *409*, 325−342.
(40) Beroll, P.; Schmalzl, S.; Volkmer, D. Influence of surface-modification, length and volume fraction of carbon short fibres on the mechanical properties of calcium aluminate cement systems. *Mater. Today Commun.* **2020**, *25*, 101704.
(41) Dong, F.; Hou, G.; Cao, F.; Yan, F.; Liu, L.; Wang, J. The lubricity and reinforcement of carbon fi bers in polyimide at high temperatures. *Tribol. Int.* **2016**, *101*, 291−300.
(42) Li, V. C.; Maalej, M. Toughening in cement based composites. Part II: Fibre reinforced cementitious composites. *Cem. Concr. Compos.* **1996**, *18*, 239−249.

https://doi.org/10.1021/acsomega.2c00617
ACS Omega 2023, 8, 1864−1875

(43) Krüger, R.; Groll, J. Biomaterials Fibre reinforced calcium phosphate cements e On the way to degradable load bearing bone substitutes? *Biomaterials* **2012**, *33*, 5887−5900.

https://doi.org/10.1021/acsomega.2c00617
ACS Omega 2023, 8, 1864−1875